



Cite this: *Sens. Diagn.*, 2023, 2, 902

Graphitic carbon nitride with Cu²⁺ and triazole group co-doping for enhanced peroxidase-like activity and its application for glutathione detection†

Xiaotao Liu, Xueyi Zheng, Chunqiu Xia and Liangqia Guo *

Nanozymes have attracted great interest in the field of biotechnology, (bio)sensing, and environmental monitoring. Herein, a co-doping strategy is proposed to enhance the peroxidase-like activity of graphitic carbon nitride (g-C₃N₄). Cu²⁺ and triazole group co-doped graphitic carbon nitride (g-C₃N₅-Cu²⁺) was derived from thermal polymerization of 3-amino-1,2,4-triazole and then coordination with Cu²⁺. g-C₃N₅-Cu²⁺ nanosheets (NSs) could catalyze the oxidation reaction of 3,3',5,5'-tetramethylbenzidine (TMB) by H₂O₂ under neutral conditions, yielding 10.9-fold better catalytic activity than g-C₃N₄ NSs. Reactive oxygen species scavenging experiments indicated that [•]OH played a crucial role during the catalytic process. When glutathione (GSH) was introduced, the absorbance of the system decreased because of the reduction of the oxidation product of TMB by GSH. The colorimetric method demonstrated a sensitive response for GSH with a linear range of 0.8–33.3 μmol L⁻¹ and a limit of detection of 0.3 μmol L⁻¹. The sensitivity is higher than most other peroxidase mimetic-based colorimetric methods for GSH. Finally, the feasibility for the detection of GSH in HeLa cells was demonstrated.

Received 31st March 2023,
Accepted 31st May 2023

DOI: 10.1039/d3sd00072a

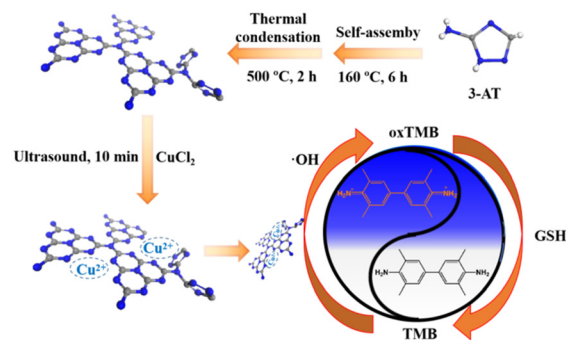
rsc.li/sensors

1. Introduction

Natural enzymes have been extensively applied in the fields of medicine, chemistry, food, environment and agriculture due to their superior catalytic efficiency and substrate specificity.¹ Nevertheless, their catalytic activities are susceptible to environmental conditions and their preparation and purification are expensive.^{2,3} To surmount the shortage of natural enzymes, nanozymes, with unique advantages including high activity and stability, low cost, and easy scaled-up and modification, have provoked wide interest in the fields of biosensing and biotherapy.^{4–6} Since 2007, when Fe₃O₄ nanoparticles were first reported to have peroxidase-like activity,⁷ more and more nanozymes have been discovered, including carbon-based nanomaterials,⁸ transition metal nanomaterials,⁹ precious metal nanomaterials, *etc.*¹⁰

Graphitic carbon nitrides (g-C₃N₄), as a carbon-based material, are of particular importance due to their distinctive properties such as high physicochemical stability, tunability

of band gaps, nontoxicity and biocompatibility.^{11–14} Since the first discovery of peroxidase-like activity,¹⁵ g-C₃N₄ as a peroxidase mimetic has attracted more and more attention. Since then, many methods such as modification of gold NPs,¹⁶ complexation of precious metal ruthenium ions,¹⁷ decoration with Au-Ni bimetallic NPs,¹⁸ functionalization of Cu²⁺ modified carbon dots,^{19,20} and hybridization of Cu (ref. 21) with g-C₃N₄ were proposed to improve its peroxidase-like activity. Despite great progress on g-C₃N₄-based peroxidase mimetics being achieved, the complex and cumbersome synthesis method,^{16–20} or the utilization of precious metals^{16–18} was involved.



Scheme 1 The preparation of g-C₃N₅-Cu²⁺ NSs and colorimetric detection of GSH.

Ministry of Education Key Laboratory for Analytical Science of Food Safety and Biology, Fujian Provincial Key Laboratory of Analysis and Detection Technology for Food Safety, College of Chemistry, Fuzhou University, Fuzhou 350116, China.
E-mail: lqguo@fzu.edu.cn

† Electronic supplementary information (ESI) available. See DOI: <https://doi.org/10.1039/d3sd00072a>



Herein, we proposed a co-doping strategy to enhance the peroxidase-like activity of g-C₃N₄. Cu²⁺ and triazole group co-doped g-C₃N₄ (denoted as g-C₃N₅-Cu²⁺) was derived from thermal polymerization of 3-amino-1,2,4-triazole (3-AT) and then coordination with Cu²⁺. The catalytic activity of the g-C₃N₅-Cu²⁺ nanozyme was 10.9-fold greater than that of g-C₃N₄. The catalytic kinetics and mechanism of the g-C₃N₅-Cu²⁺ nanozyme were investigated by steady-state kinetic experiments and reactive oxygen species (ROS) scavenging experiments, respectively. Finally, the g-C₃N₅-Cu²⁺ nanozyme was applied for the colorimetric detection of glutathione (GSH) in HeLa cells (Scheme 1).

2. Experimental

2.1. Chemical and materials

3-AT, cupric chloride (CuCl₂), NaN₃, GSH, methionine (Met), histidine (His), alanine (Ala), glycine (Gly), glutamate (Glu), cystine (Cys) and phenylalanine (Phe) were obtained from Sangon Biotech (Shanghai) Co., Ltd. Hydrogen peroxide (H₂O₂), disodium oxalate (Na₂C₂O₄), terephthalic acid (TA), thiourea, and 3,3',5,5'-tetramethylbenzidine (TMB) were bought from Aladdin Co., Ltd. Superoxide dismutase (SOD) was purchased from Worthington Biochemical Corporation. The commercial GSH kit was provided by Beyotime Biotechnology Co., Ltd.

2.2. Preparation of g-C₃N₅-Cu²⁺ nanosheets

Under N₂ atmosphere, 2 g 3-AT was self-assembled at 160 °C for 6 h, and then polymerized at 500 °C for 2 h. After cooling, 0.2 g g-C₃N₅ powder was treated ultrasonically in 50 mL water for 24 h. The precipitation between 8000 rpm to 12 000 rpm was collected. After re-dispersion of the precipitate in water, the concentration of g-C₃N₅ NSs was adjusted to 1.0 mg mL⁻¹. Similarly, g-C₃N₄ NSs were obtained *via* thermal polymerization of melamine¹⁵ and then ultrasonic exfoliation.

To 3 mL g-C₃N₅ NSs (1.0 mg mL⁻¹), 1 mL CuCl₂ solution (16 mmol L⁻¹) was added. After ultrasonic treatment for 10 min, free Cu²⁺ in the mixture was removed by washing with water. The dispersion of g-C₃N₅-Cu²⁺ NSs was adjusted to 1.0 mg mL⁻¹. Similarly, g-C₃N₄-Cu²⁺ NSs were also prepared.

2.3. Colorimetric detection of GSH

To 200 µL of Tris-HCl buffer (50 mmol L⁻¹, pH 6.5), 50 µL of TMB (10 mmol L⁻¹), 50 µL of g-C₃N₅-Cu²⁺ NSs (1.0 mg L⁻¹), 200 µL of H₂O₂ (400 µmol L⁻¹) and 100 µL of GSH with different concentrations were added. After incubation at 50 °C for 50 min, g-C₃N₅-Cu²⁺ NSs was removed from the mixture by centrifugation. The absorption spectrum of the mixture was recorded.

3. Results and discussion

3.1. Characterization of g-C₃N₅-Cu²⁺ nanosheets

g-C₃N₅-Cu²⁺ NSs were derived from thermal polymerization of 3-AT at 500 °C under nitrogen atmosphere and then coordination with Cu²⁺. 3-AT was chosen as the precursor, which can incorporate triazole groups into g-C₃N₄ after thermal condensation.²² As shown in the TEM image (Fig. 1A), the lateral size of g-C₃N₅-Cu²⁺ NSs is less than 150 nm. The most probable size distribution of g-C₃N₅-Cu²⁺ NSs is about 165 nm (Fig. S1A†). In the XRD patterns (Fig. 1B), the peak assigned to the (002) plane of g-C₃N₅-Cu²⁺ exhibits a right-shift from 27.4° to 27.6° after doping with Cu²⁺, which may be caused by the crystal lattice distortion after Cu²⁺ coordination.²³ The diffraction peak at 13.3° disappears, indicating the decreasing size of the conjugate plane.²⁴ In the FT-IR spectra (Fig. 1C), the peaks at 803 cm⁻¹ and 1245–1635 cm⁻¹ feature the typical absorption of (tri-*s*)triazine ring and aromatic carbon nitride heterocyclic ring, respectively.^{25,26} It's worth noting that there is a peak in 1425 cm⁻¹ which belongs to the ring breathing modes of triazole groups.²² The above results indicate that there are triazole groups in the carbon nitride network. As observed from the survey XPS spectrum (Fig. 1D), g-C₃N₅-Cu²⁺ NSs are composed of C, N, O and Cu elements. The presence of the O element may be ascribed to the adsorption of H₂O and O₂ in the air on the surface of the material.²⁷ The atom ratio of C/N in g-C₃N₅-Cu²⁺ NSs was calculated to be 3:4.7, which is higher than the ratio in g-C₃N₄ NSs.²⁸ Due to the low content of Cu²⁺, the Cu element does not appear in the survey spectrum. In the C 1s core-level spectrum there are four peaks with binding energies (BEs) of 284.6, 286.1, 288.1, and 289 eV (Fig. 1E), which belong to the adventitious carbon (adv. C), C–N, N=C–N₂, and C–NH₂, respectively. There are three peaks with BEs of 398.6, 400, 404.8 eV in the N 1s core-level spectrum (Fig. 1F), which belong to C=N=C, N–(C)₃, and the heterocyclic compound charge effect or positive charge delocalization (π–π*), respectively. In the Cu 2p core-level XPS spectrum of g-C₃N₅-Cu²⁺ NSs (Fig. S1B†), there are three peaks at 932.3 eV, 942.0 eV and 952.3 eV, corresponding to Cu 2p_{3/2}, satellite and Cu 2p_{1/2} characteristic peaks of Cu²⁺,²⁹ indicating the adsorption of Cu²⁺ in g-C₃N₅ NSs. The energy-dispersive spectroscopy (EDS) mapping in Fig. S1C–F† further confirms that the C, N, O, Cu atoms are well distributed in the frameworks of g-C₃N₅-Cu²⁺ NSs; the mass of Cu in g-C₃N₅-Cu²⁺ NSs is about 1.4% by ICP-MS. For comparison, g-C₃N₄-Cu²⁺ NSs were also characterized in Fig. S2 and S3.† The morphology and chemical components of g-C₃N₄-Cu²⁺ NSs are similar with g-C₃N₅-Cu²⁺ NSs except for the absence of triazole groups.

3.2. Peroxidase-like activity of g-C₃N₅-Cu²⁺ nanosheets

The peroxidase-like activity of g-C₃N₅-Cu²⁺ NSs was studied with TMB as the substrate. When TMB was mixed with g-



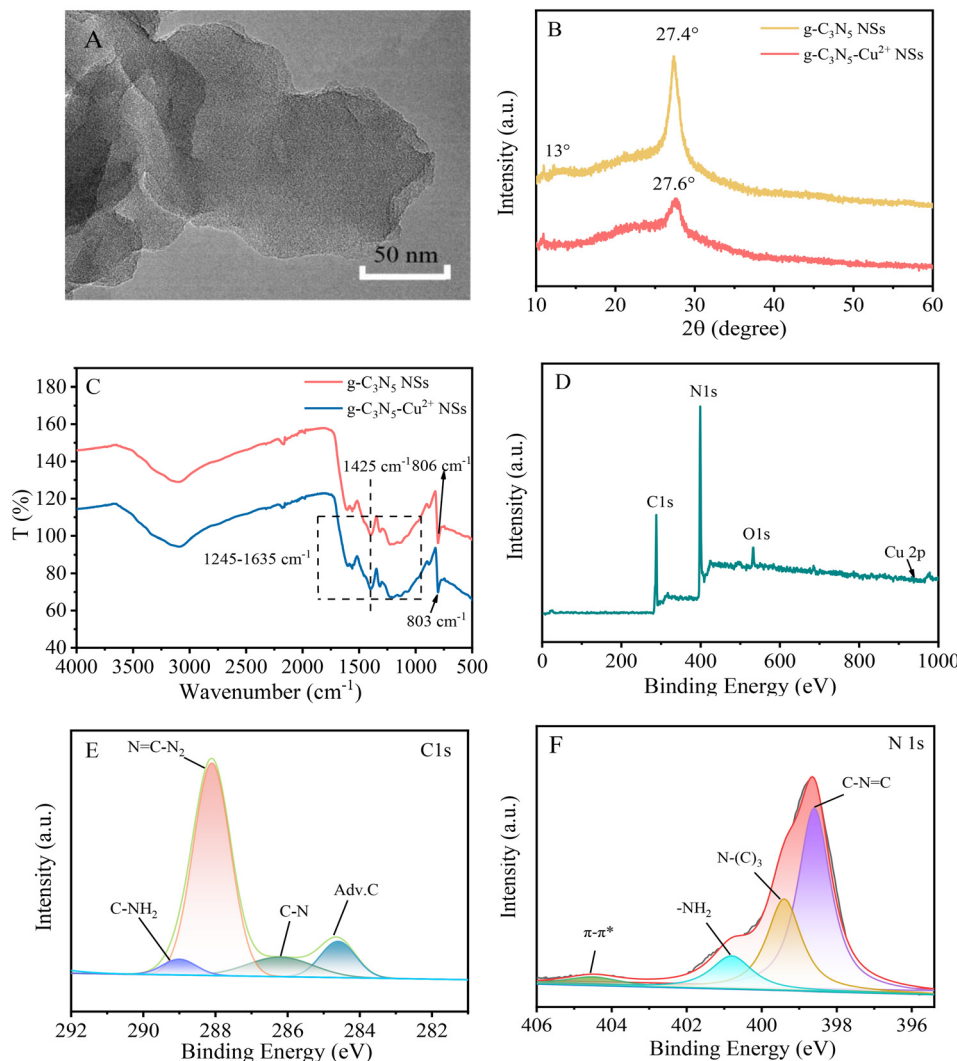


Fig. 1 TEM image of $g\text{-C}_3\text{N}_5\text{-Cu}^{2+}$ NSs (A), XRD patterns (B) and FT-IR spectra (C) of $g\text{-C}_3\text{N}_5$ and $g\text{-C}_3\text{N}_5\text{-Cu}^{2+}$ NSs, and survey (D), C 1s core-level (E) and N 1s core-level (F) XPS spectra of $g\text{-C}_3\text{N}_5\text{-Cu}^{2+}$ NSs.

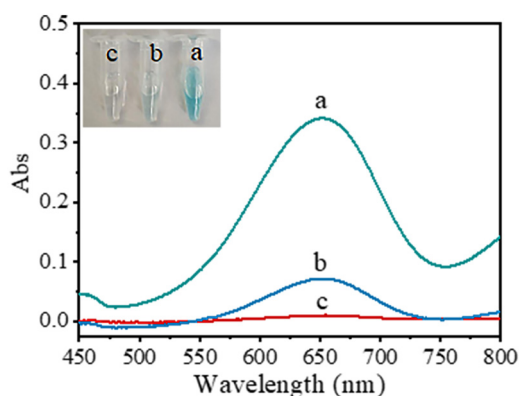


Fig. 2 Absorption spectra of TMB solution on addition of $g\text{-C}_3\text{N}_5\text{-Cu}^{2+}$ NSs and H_2O_2 (a), H_2O_2 (b), and $g\text{-C}_3\text{N}_5\text{-Cu}^{2+}$ NSs (c), respectively. Conditions: Tris-HCl (pH 3, 50 mmol L^{-1}), $g\text{-C}_3\text{N}_5\text{-Cu}^{2+}$ NSs (0.1 mg mL^{-1}), TMB (1.2 mmol L^{-1}), H_2O_2 (80 $\mu\text{mol L}^{-1}$), reaction temperature (37 $^\circ\text{C}$), incubating time (30 min). Inset are photos of the mixed solution.

$\text{C}_3\text{N}_5\text{-Cu}^{2+}$ NSs and H_2O_2 , the mixed solution turned to a blue color. A typical absorption peak at 652 nm originating from the oxidation product of TMB (oxTMB) is observed (line a Fig. 2a). However, without $g\text{-C}_3\text{N}_5\text{-Cu}^{2+}$ NSs or H_2O_2 , the color of the mixed solutions does not change (lines b and c in Fig. 2a). These results indicate that $g\text{-C}_3\text{N}_5\text{-Cu}^{2+}$ NSs catalyze the oxidation of TMB by H_2O_2 , revealing their peroxidase-like activity. The effect of the concentration of Cu^{2+} coordinated with $g\text{-C}_3\text{N}_5$ NSs on the catalytic activity was investigated (Fig. S4†). The catalytic activity of $g\text{-C}_3\text{N}_5\text{-Cu}^{2+}$ NSs is enhanced with the increase of Cu^{2+} concentration and reaches a peak at 4 mmol L^{-1} Cu^{2+} .

To prove the vital role of Cu^{2+} and triazole groups on the catalytic activity of $g\text{-C}_3\text{N}_5\text{-Cu}^{2+}$ NSs, the catalytic activities of $g\text{-C}_3\text{N}_5\text{-Cu}^{2+}$, $g\text{-C}_3\text{N}_4\text{-Cu}^{2+}$ NSs, $g\text{-C}_3\text{N}_5$ NSs, and $g\text{-C}_3\text{N}_4$ NSs were compared. As shown in Fig. 3, the peroxidase-like activity is in the order of $g\text{-C}_3\text{N}_5\text{-Cu}^{2+}$ NSs > $g\text{-C}_3\text{N}_4\text{-Cu}^{2+}$ NSs > $g\text{-C}_3\text{N}_5$ NSs > $g\text{-C}_3\text{N}_4$ NSs. The catalytic activity of $g\text{-C}_3\text{N}_5\text{-Cu}^{2+}$ NSs is 3.4-fold greater than that of $g\text{-C}_3\text{N}_4\text{-Cu}^{2+}$ NSs, 7.2-



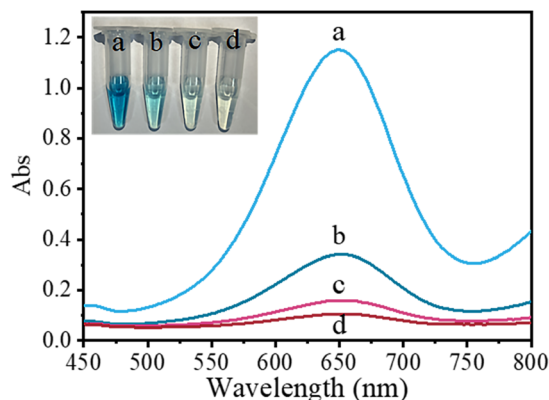


Fig. 3 Absorption spectra of TMB solution on addition of g-C₃N₅-Cu²⁺ NSs and H₂O₂ (a), g-C₃N₄-Cu²⁺ NSs and H₂O₂ (b), g-C₃N₅ NSs and H₂O₂ (c), and g-C₃N₄ NSs and H₂O₂ (d), respectively. Conditions: g-C₃N₅-Cu²⁺ NSs (0.1 mg mL⁻¹), g-C₃N₄-Cu²⁺ NSs (1 mg L⁻¹), g-C₃N₅ NSs (0.1 mg mL⁻¹), g-C₃N₄ NSs (0.1 mg mL⁻¹), TMB (1.0 mmol L⁻¹), H₂O₂ (80 μmol L⁻¹), reaction temperature (50 °C), incubating time (50 min).

fold greater than that of g-C₃N₅ NSs and 10.9-fold greater than that of g-C₃N₄ NSs. These phenomena indicate that Cu²⁺ and triazole groups synergistically boost the peroxidase-like activity of g-C₃N₄ NSs.

3.3. Catalytic kinetics and mechanism

To investigate the catalytic performance of g-C₃N₅-Cu²⁺ NSs, the steady-state kinetics of g-C₃N₅-Cu²⁺ NSs was investigated (Fig. S5†). The catalytic reactions between g-C₃N₅-Cu²⁺ NSs and TMB, and between g-C₃N₅-Cu²⁺ NSs and H₂O₂ followed the typical Michaelis-Menten behavior. The maximal reaction velocity (V_{\max}) as well as the Michaelis-Menten constant (K_m) was deduced from the Lineweaver-Burk plot. The V_{\max} value of g-C₃N₅-Cu²⁺ NSs for the

substrate H₂O₂ was calculated to be 1.8×10^{-6} mol L⁻¹ s and is higher than those of HRP and some other peroxidase mimetics (Table S1†).^{15,30–32} These results indicated that g-C₃N₅-Cu²⁺ NSs showed a higher reaction rate for the substrate H₂O₂ than those of HRP and some other peroxidase mimetics.

The catalytic mechanism of g-C₃N₅-Cu²⁺ NSs was further investigated by reactive oxygen species scavengers. Three concentrations of thiourea, NaN₃, SOD, and NaC₂O₄ were used to capture [•]OH, ¹O₂, [•]O²⁻ and H₂O₂, respectively.^{33,34} As shown in Fig. 4A, NaN₃ and SOD have almost no effect on the catalytic reaction, indicating that ¹O₂ and [•]O²⁻ are not produced during the catalytic reaction. However, with the increasing concentration of thiourea and NaC₂O₄, the absorbance of the system gradually decreased, indicating that [•]OH and H₂O₂ play a crucial role in the catalytic reaction. To further confirm the production of [•]OH in the system, TA was commonly used to verify the presence of [•]OH (Fig. 4B). [•]OH can oxidize TA to generate strongly fluorescent 2-hydroxyterephthalic acid.³⁵ In the presence of only H₂O₂, the fluorescence signal is very low. However, the fluorescence signal is significantly enhanced in the presence of both g-C₃N₅-Cu²⁺ NSs and H₂O₂. The results further verified that [•]OH are produced in the systems. From these results we can infer that g-C₃N₅-Cu²⁺ NSs catalyze H₂O₂ to form [•]OH, which oxidizes TMB to oxTMB.

3.4. Colorimetric detection of H₂O₂ and GSH

The effects of pH, g-C₃N₅-Cu²⁺ NS concentration, TMB concentration, incubation time, and reaction temperature on the absorbance of the system were first investigated. The experimental conditions were optimized at pH 6.5, 50 °C reaction temperature, 0.1 mg mL⁻¹ g-C₃N₅-Cu²⁺ NSs and 1.0 mmol L⁻¹ TMB (Fig. S6†). It is worth mentioning that g-C₃N₅-Cu²⁺ NSs can maintain relatively high catalytic activity over a wide pH range (2.0 to 6.5), which is beneficial for its

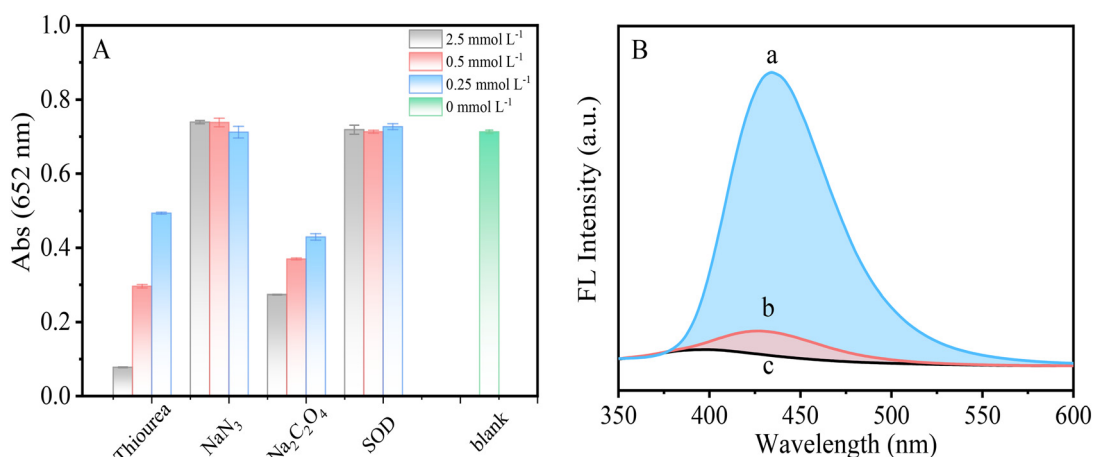


Fig. 4 (A) Effect of different scavengers on the absorbance of the system. (B) Fluorescence spectra of TA (1 mmol L⁻¹) with the coexistence of H₂O₂ (1.0 mmol L⁻¹) and g-C₃N₅-Cu²⁺ NSs (0.1 mg mL⁻¹) (a), H₂O₂ (1.0 mmol L⁻¹) (b), and g-C₃N₅-Cu²⁺ NSs (0.1 mg mL⁻¹) (c), respectively.

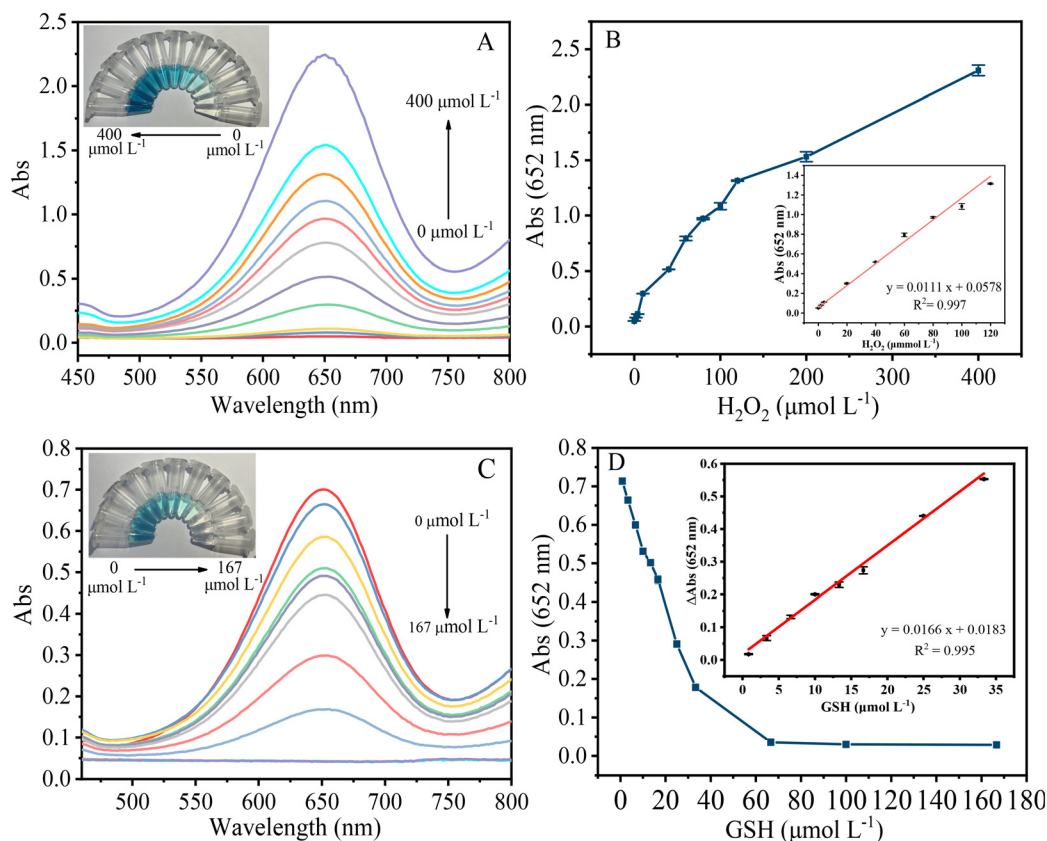


Fig. 5 (A) Absorption spectra of the mixed solutions with different concentrations of H_2O_2 (0–400 $\mu\text{mol L}^{-1}$). Inset shows the color of the mixed solution. (B) The absorbance at 652 nm vs. H_2O_2 concentration. Inset is the calibration curve for H_2O_2 . (C) Absorption spectra of the mixed solutions with different concentrations of GSH (0–167 $\mu\text{mol L}^{-1}$). Inset shows the color of the mixed solution. (D) The absorbance at 652 nm vs. GSH concentration. Inset is the calibration curve for GSH.

application. This high peroxidase-like activity of $\text{g-C}_3\text{N}_5\text{-Cu}^{2+}$ NSs over a wide pH may be explained by the triazole groups in $\text{g-C}_3\text{N}_5\text{-Cu}^{2+}$ NSs favoring the adsorption of TMB molecules *via* π - π stacking.

Thus, a facile colorimetric method for H_2O_2 was constructed *via* the $\text{g-C}_3\text{N}_5\text{-Cu}^{2+}$ NSs-TMB system. The absorbance is gradually enhanced with the increase of H_2O_2 concentration (Fig. 5A). There is a linear range between the absorbance and H_2O_2 over 0–120 $\mu\text{mol L}^{-1}$ (Fig. 5B). The limit of detection (LOD) of 0.32 $\mu\text{mol L}^{-1}$ was achieved by $3\sigma/k$, where σ and k are the standard deviation of 12 repeated detections of the blank solution and the slope of the linear equation, respectively. $\text{g-C}_3\text{N}_5\text{-Cu}^{2+}$ NSs were further applied to construct a colorimetric method for GSH *via* the reduction of oxTMB. The absorbance gradually dropped with the increase of GSH concentration (Fig. 5C). The blue color of the mixed solution gradually fades. The linear detection range for GSH over 0.8–33.3 $\mu\text{mol L}^{-1}$ is obtained (Fig. 5D). The LOD for GSH is calculated to be 0.25 $\mu\text{mol L}^{-1}$ by $3\sigma/k$. As shown in Table S2,† the LOD is lower than those colorimetric methods catalyzed by other peroxidase mimetics such as carbon nanodots,³⁶ CuS-polydopamine-Au composites,³⁷ Fe-Ne-C single atom nanozymes,³⁸ carbon nanoparticles,³⁹ etc.

3.5. Selectivity toward GSH

To probe the selectivity of this colorimetric method for GSH, the absorbance changes on addition of possible interferences such as Met, His, Ala, Gly, Glu, Cys, and Phe were compared with that of GSH. The concentration of GSH and Cys was set to 16.7 $\mu\text{mol L}^{-1}$ while other amino acids were set to 10-fold concentrations of GSH. Little absorbance change was observed except for GSH and Cys (Fig. S7†). Although Cys can cause relatively large absorbance changes with GSH, the concentration of Cys (about 60–200 $\mu\text{mol L}^{-1}$) in cells is much lower than that of GSH (about 1–10 mmol L^{-1}).⁴⁰ When cellular GSH level was detected, the dilution of cell lysate can overcome the interference caused by Cys.

3.6. Application

The colorimetric method was applied for the detection of GSH in HeLa cells. Cell culture and pretreatment details of HeLa cells are provided in the ESI.† The results are listed in Table S3.† The GSH concentration in the lysate of HeLa cells was measured as 4.6 mmol L^{-1} by the colorimetric method, close to the value (5.2 mmol L^{-1}) assayed by the commercial GSH assay kit (Fig. S8†). This colorimetric method also



demonstrated excellent recovery (100.4–103%) and relative standard derivation (0.6–2.1%) for the detection of GSH in cell lysate.

4. Conclusions

$g-C_3N_5-Cu^{2+}$ NSs were successfully prepared by thermal polymerization of 3-AT and coordination with Cu^{2+} . The catalytic activity of $g-C_3N_5-Cu^{2+}$ NSs is 3.4-fold greater than that of $g-C_3N_4-Cu^{2+}$ NSs without triazole groups, and 10.9-fold greater than that of $g-C_3N_4$. The study of the catalytic mechanism reveals that 'OH plays a crucial role during the catalytic process. Finally, $g-C_3N_5-Cu^{2+}$ NSs were utilized to construct a sensitive and selective detection method for GSH in cell lysate. This study exploited a new strategy to rationally design effective bio-inspired nanozymes. It is envisioned that $g-C_3N_5-Cu^{2+}$ NSs hold great potential to replace horseradish peroxidase for chemical sensing and biotechnology applications.

Author contributions

Xiaotao Liu: conceptualization, methodology, investigation, and writing – original draft. Xueyi Zheng: validation and investigation. Chunqiu Xia: validation and investigation. Liangqia Guo: conceptualization, funding acquisition, supervision, writing – review & editing.

Conflicts of interest

There are no conflicts to declare.

Acknowledgements

This work was supported by the National Natural Science Foundation of China (No. 21874023, 22176034).

Notes and references

- G. Wulff, *Chem. Rev.*, 2001, **102**, 1–28.
- A. Ashraf, Z. Bytesnikova, J. Barek, L. Richtera and V. Adam, *Biosens. Bioelectron.*, 2021, **19**, 113494.
- J. Xie, X. Zhang, H. Wang, H. Zheng and Y. Huang, *TrAC, Trends Anal. Chem.*, 2012, **39**, 114–129.
- D. Jiang, D. Ni, Z. Rosenkrans, P. Huang, X. Yan and W. Cai, *Chem. Soc. Rev.*, 2019, **48**, 3683–3704.
- J. Wu, X. Wang, Q. Wang, Z. Lou, S. Li, Y. Zhu, L. Qin and H. Wei, *Chem. Soc. Rev.*, 2019, **48**(4), 1004–1076.
- Y. Huang, J. Ren and X. Qu, *Chem. Rev.*, 2019, **119**(6), 4357–4412.
- L. Gao, J. Zhuang, L. Nie, J. Zhang, Y. Zhang, N. Gu, T. Wang, J. Feng, D. Yang, S. Perrett and X. Yan, *Nat. Nanotechnol.*, 2007, **2**, 577.
- P. Zhang, D. Sun, A. Cho, S. Weon, S. Lee, J. Lee, J. Han, D. Kim and W. Choi, *Nat. Commun.*, 2019, **10**, 940.
- Y. Sang, Y. Huang, W. Li, J. Ren and X. Qu, *Chem. – Eur. J.*, 2018, **24**(28), 7259–7263.

- Y. Xu, J. Fei, G. Li, T. Yuan, X. Xu and J. Li, *Angew. Chem., Int. Ed.*, 2019, **58**(17), 5572–5576.
- S. Cao, J. Low, J. Yu and M. Jaroniec, *Adv. Mater.*, 2015, **27**(13), 2150–2176.
- Q. Hao, G. Jia, W. Wei, A. Vinu, Y. Wang, H. Arandiyan and B. Ni, *Nano Res.*, 2020, **13**, 18–37.
- Z. Zhou, Y. Zhang, Y. Shen, S. Liu and Y. Zhang, *Chem. Soc. Rev.*, 2018, **47**, 2298–2321.
- Y. Dong, Q. Wang, H. Wu, Y. Chen, C. Lu, Y. Chi and H. Yang, *Small*, 2016, **12**(39), 5376–5393.
- T. Lin, L. Zhong, J. Wang, L. Guo, H. Wu, Q. Guo, F. Fu and G. Chen, *Biosens. Bioelectron.*, 2014, **59**, 89–93.
- N. Wu, Y. Wang, F. Guo, H. Wen, T. Yang and J. Wang, *Anal. Chim. Acta*, 2019, **1091**, 69–75.
- W. Den, Y. Peng, H. Yang, Y. Tan, M. Ma, Q. Xie and S. Chen, *ACS Appl. Mater. Interfaces*, 2019, **11**(32), 29072–29077.
- G. Darabdhara, J. Bordoloi, P. Manna and M. Das, *Sens. Actuators, B*, 2019, **285**, 277–290.
- M. González, W. Liao, R. Cazelles, S. Wang, X. Yu, V. Gutkin and I. Willner, *ACS Nano*, 2017, **11**, 3247–3253.
- Q. Li, D. Yang, Q. Yin, W. Li and Y. Yang, *ACS Appl. Nano Mater.*, 2022, **5**, 1925–1934.
- T. Dang, N. Heo, H. Cho, S. Lee, M. Song, H. Kim and M. Kim, *Microchim. Acta*, 2021, **188**, 293.
- G. Man, S. Talapaneni, K. Lakhi, H. Ilbeygi, U. Ravon, K. Bahily, T. Mori, D. Park and A. Vinu, *Angew. Chem., Int. Ed.*, 2017, **56**, 848–8485.
- S. Hu, X. Qu, J. Bai, P. Li, Q. Li, F. Wang and L. Song, *ACS Sustainable Chem. Eng.*, 2017, **5**, 6863–6872.
- C. Huang, Y. Wen, J. Ma, D. Dong, Y. Shen, S. Liu, H. Ma and Y. Zhang, *Nat. Commun.*, 2021, **12**, 320.
- Z. Song, T. Lin, L. Lin, S. Lin, F. Fu, X. Wang and L. Guo, *Angew. Chem., Int. Ed.*, 2016, **55**, 2773–2777.
- X. Wang, S. Blechert and M. Antonietti, *ACS Catal.*, 2012, **2**, 1596–1606.
- X. Liu, H. Zhang, Z. Cai and L. Guo, *Spectrochim. Acta, Part A*, 2022, **268**, 120685.
- W. Ong, L. Tian, Y. Ng, S. Yong and S. Chai, *Chem. Rev.*, 2016, **116**(12), 7159–7329.
- C. Y. Hu, Z. W. Jiang, C. Z. Huang and Y. F. Li, *Microchim. Acta*, 2021, **188**, 272.
- N. Wu, Y. Wang, X. Wang, F. Guo, H. Wen, T. Yang and J. Wang, *Anal. Chim. Acta*, 2019, **1091**, 69–75.
- G. Darabdhara, J. Bordoloi, P. Manna and M. Das, *Sens. Actuators, B*, 2019, **285**, 277–290.
- T. Dang, N. Heo, H. Cho, S. Lee, M. Song, H. Kim and M. Kim, *Microchim. Acta*, 2021, **188**, 293.
- C. Liu, D. Kong, P. Hsu, H. Yuan, H. Lee, Y. Liu, H. Wang, S. Wang, K. Yan and D. Lin, *Nat. Nanotechnol.*, 2016, **11**, 1098–1104.
- C. Lu, F. Zhou, S. Wu, L. Liu and D. Xing, *Antioxid. Redox Signaling*, 2016, **24**, 249–262.
- Y. Li, T. Li, W. Chen and Y. Song, *ACS Appl. Mater. Interfaces*, 2017, **9**, 29881–29888.
- M. Shamsipur, A. Safavi and Z. Mohammadpour, *Sens. Actuators, B*, 2014, **199**, 463–469.



- 37 Y. Wang, Y. Liu, F. Ding, X. Zhu, L. Yang, P. Zou, H. Rao, Q. Zhao and X. Wang, *Anal. Bioanal. Chem.*, 2018, **410**, 4805–4813.
- 38 W. Lu, S. Chen, H. Zhang, J. Qiu and X. Liu, *J. Materiomics*, 2022, **23**, 52–8478.
- 39 L. Chen, X. Li, Z. Li, K. Liu and J. Xie, *RSC Adv.*, 2022, **12**, 595–601.
- 40 Y. Yue, F. Huo, P. Ning, Y. Zhang, J. Chao, X. Meng and C. Yin, *J. Am. Chem. Soc.*, 2017, **139**, 3181–3185.

